# High power continuous wave laser heating of graphite in a high temperature range up to 3800 K

L. Gallais, T. Vidal, E. Lescoute, Y. Pontillon, J. Rullier

# High power continuous wave laser heating of Graphite in a high temperature range up to 3800K.

L. Gallais[1,*], T. Vidal[1], E. Lescoute[2], Y. Pontillon[3], J.L. Rullier[4]

[1]Aix Marseille Univ, CNRS, Centrale Marseille, Institut Fresnel, 13013 Marseille, France

[2]CEA DIF, Bruyères-le-Châtel, 91297 Arpajon, France

[3]CEA, DES, IRESNE, DEC, Cadarache, 13115 Saint-Paul-Lez-Durance, France

[4]CEA CESTA, 15 Avenue des Sablières, 33114 Le Barp, France

*email adress : laurent.gallais@fresnel.fr

Abstract

As graphite is an important material for several applications, the evaluation of its properties at very high temperature is of major importance. Conducting studies at temperature > 2800K is however very challenging and the amount of available data in the literature is therefore very limited. This paper presents a methodology that compares experimental data to simulation results following a progressive increase of the temperature range investigated. The study was conducted on a commercial polycrystalline graphite produced by sintering (EDM3 from POCO) under high power continuous laser heating (kW Ytterbium at a wavelength of 1080 nm). Experiments were done inside a vacuum chamber equipped with pyrometers and cameras allowing fine monitoring of the temperature of the samples. A 3D numerical model has been developed based on the Finite Element Method to analyse the experimental results. The evolution of thermal and optical properties of EDM3 with temperature are required for modelling correctly the laser / material Interaction. By running sequential comparison of calculation with dedicated experiment we achieve better knowledge of such properties. From this study we obtain estimations of the evolution of thermal conductivity, emissivity and evaporation rate up to 3800 K of amorphous graphite.

# I Introduction

Graphite is an important material for scientific and industrial applications because of some of its peculiar properties: it is extremely resistant to heat, nearly inert when put in contact with almost any other material, and has good thermal and electrical conductivity. Its refractory properties in combination with its mechanical properties make it a material of choice in very demanding applications in the nuclear or aerospace industries: it is used for instance as a neutron moderator within fission graphite-based nuclear reactors [1-3], as plasma facing walls in nuclear fusion experimental reactors [4-6], or atmospheric reentry surfaces of aircrafts [7]. In such applications, the knowledge of the material properties (thermal, mechanical, optical) at very high temperature (close to the sublimation point of approximately 3900 K at atmospheric pressures or below [8]) is of critical importance. However, conducting studies at such high temperatures can be very challenging and the amount of available data is therefore very limited. For such studies, laser techniques are particularly suitable since they can easily drive materials to extreme temperatures with a very high amount of precision and control. They can be combined with contactless instruments (pyrometry, spectrometry, thermal imaging) to derive the thermophysical properties of materials. Such an approach based on the analysis of laser-based temperature to extract temperature-dependent materials properties was for instance applied by Combis et al [9] or Elhadj et al [10] to determine fused silica thermal diffusivity, conductivity and specific heat up to 3000 K. Their work demonstrate that these methods of local laser heating combined to contactless thermal measurements methods can be reliable, and useful to study materials under extreme conditions, which often remain out of reach of conventional methods. The approach is however not without technical and analytical challenges: in particular the non-isothermal conditions inherent to laser heating can make interpretation of results difficult.

In this context, we present in this work our contribution to obtain a better knowledge of the behaviour and properties of amorphous graphite in the very high temperature range (2800-3800 K). Such properties include thermal conductivity and diffusivity, spectral emissivity as well as a

thermodynamical description of mass loss close to the sublimation point. For that purpose, we have developed and used experimental systems involving high power lasers (1-2 kW) operating at 1.08 µm, that take benefit of the high absorption coefficient of graphite at this wavelength. This allows us to heat samples (EDM-3 grade from POCO Company) very locally in well-controlled conditions up to 3800 K. We then obtain the temperature evolution during different parametric studies. These results are compared with simulations from a numerical model that we have developed based on the Finite Element Method (under COMSOL software). Following this analysis, it is possible to obtain a better knowledge of the laser-graphite interactions at high temperature with estimations of the evolution of thermal parameters, emissivity, laser absorption and evaporation rate.

In part II of this paper we detail the experimental techniques and methods. The numerical model and associated material parameters are then described in part III. Finally, results obtained based on these experimental and numerical tools are presented and discussed in part IV, going progressively from elevated temperature (ambient to 1500 K) to high temperature (1500-2800 K) and to very-high temperatures (2800-3800 K), according to classification of ‘‘high-temperatures’’ [11].

## II Experiments

### a-Materials

The work focuses on a particular material, graphite, and more specifically on EDM-3 from POCO Graphite Inc., which is a polycrystalline graphite produced by sintering. This material is used mainly for its electrical properties as an electrode for Electrical Discharge Machining (EDM) process. There are different grades of EDM graphite with significantly different properties, mainly related to the microstructure. EDM-3 is one of the so-called "Ultrafine" versions, characterized by an average grain size of less than 5 microns. It has a porosity of about 20% and it is macroscopically homogeneous with a high degree of isotropy. Aside from one sample instrumented with thermocouples, all samples used in this work are disks of 30 mm diameter with a thickness of 3, 5 or 10 mm (pictures provided in next sections). No specified surface finishing has been done on the samples surfaces but their roughness

has been measured on a VEECO profilometer with a submicrometer axial resolution. Some undesirable residues from machining were first undesirably observed, but laser annealing was sufficient to clean the samples. The sample absorption at the laser wavelength has also been evaluated. To do so, the reflectance (R) of the samples has been measured at ambient temperature using a spectrophotometer associated to an integrated sphere. The measurements were done before and after samples annealing, and a decrease of the reflection coefficient was observed after laser annealing (about 10%) that was attributed to surface cleaning. From these measurements the absorption (A=1-R) was determined to be 91.5±0.5% on the cleaned surface, the uncertainty being related to variations associated to the surface microstructure.

### b-Experimental conditions

The objective of our work is the study of graphite at high temperature, under conditions that can be reached by high power Continuous Wave (CW) laser exposure. The porous graphite under study is highly absorbing in the visible to infrared range and therefore the choice of laser wavelength can be made independently of the material. In this study we have worked with an Ytterbium fiber laser (wavelength of 1080 nm). In order to obtain exploitable results, it is necessary to heat millimetric to centimetric areas on the sample surface to have suitably homogenous temperature: this is a requirement for instance to observe the thermal gradients with a thermal camera with sufficient spatial resolution, or to assume the temperature homogeneous in the field of view of a pyrometer. However, as the heated area gets larger, the complexity in terms of thermal management and cost in term of laser power also increase. In this work we used 1-2 kW fiber lasers and beam diameters in the range 4- 13 mm.

In addition to these requirements about the laser parameters, the experiments have to be conducted in a vacuum environment in order to reduce possible oxidation of carbon by oxygen, which is highly temperature dependent [12].

### c- Experimental configuration

The experiments were conducted on the ChauCoLase platform (Chauffage Controlé par Laser / laser controlled heating) available at the Institut Fresnel [13,14], and on the GCLT facility (Générateur de Chocs Laser Transportable) located at the CEA-DIF [15].

The ChauCoLase experiment is based on a high power CW Ytterbium fiber laser (SPI laser Qube 1500) which can deliver 1500 W of maximum power with a monomode laser beam and with typical rising time of few microseconds. The beam is intrinsically not-polarized and it has a central wavelength of 1080 nm with bandwidth < 4 nm. The laser beam diameter on the sample surface can be adjusted between 4 and 13 mm (Gaussian distribution with diameter defined at $1/e^2$) by using a collimator and lens combination.

The GCLT experiment is also based on a high power CW Ytterbium fiber laser (SPI laser Qube 2000) which can deliver 2000 W of maximum power with a multimode laser beam. The laser beam diameter on the sample surface was set to 4.0 mm by means of a collimator and lens combination at a fixed position (diameter defined at $1/e^2$), and was having a super-Gaussian intensity profile (super-Gaussian function of power 6).

Common to both experiments is the fact that the laser beam can be sent through laser windows in a dedicated vacuum chamber, at normal incidence or with an angle of 40° (GCLT) or 45° (ChauCoLase) with respect to the surface. The pressure in each experimental chamber was close to $5x10^{-2}$ mbar, and the sample of interest was placed at the center of the chamber on a sample holder made of high temperature insulating material ($ZrO_2$ support to hold the sample in vertical position).

Different optical instruments were deployed to monitor and control the sample temperature through different viewports of the experimental chambers. A typical arrangement for the experiments is shown in Fig. 1, but the conditions of this study are not restricted to this arrangement.

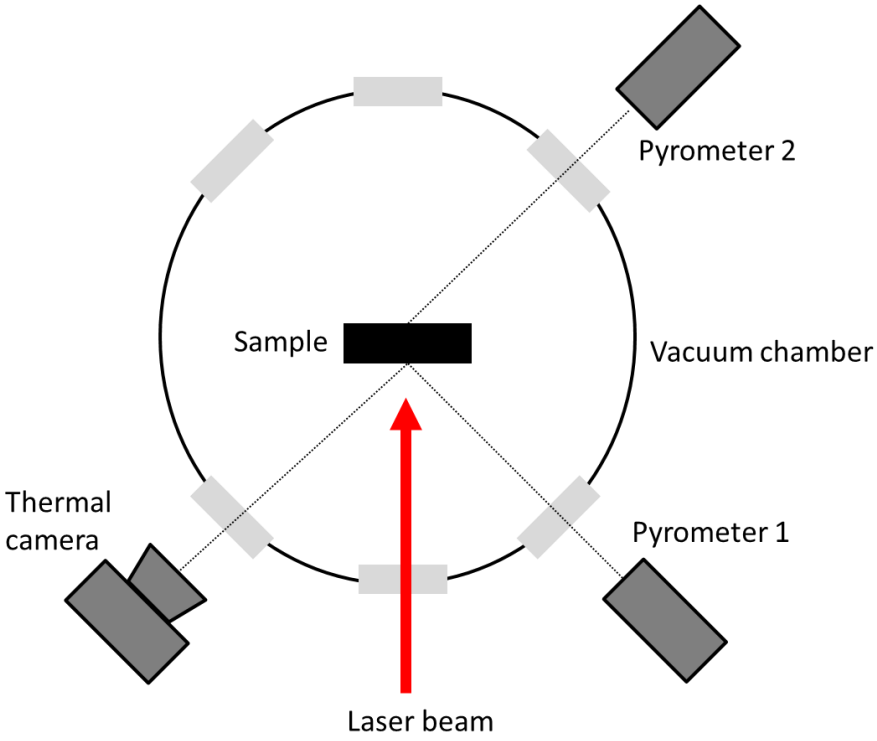


*Figure 1: Schematic of an experimental configuration*

## d- Temperature measurements and control

The different instruments used in this work to measure the temperature were common to both experiments and are:

- an infrared camera (FLIR, model A655sc) operating in the 7-14 µm band, with 300 to 2300 K range, associated to a Ge window,

- a monochromatic pyrometer (SensorTherm, model Metis M313) working at 1.27 µm for measurements in the 900-3800 K range,

- a bichromatic pyrometer (SensorTherm, model Metis H322) operating in the bands 1.45-1.65 µm and 1.65-1.8 µm for measurements in the 850-1700 K range,

- a second bichromatic pyrometer (SensorTherm, model Metis H322) operating at 1.4 and 1.64 µm for measurements in the 1600-3300 K range,

- Type K thermocouples with dedicated vacuum feedthroughs for measurements in the range 300-1500 K. They were only used for some samples equipped with holes where the thermocouples could be inserted and glued with specific adhesives, for calibration purposes (see Figure 8).

All pyrometers used have a high optical resolution, and in our set-up the measurement spot size on the sample has a diameter of 0.8 mm, and a time response below 1 ms. They were associated to a fused silica window with antireflective coating as chamber viewports. An integrated laser pointer ensures that the measurement spot size is positioned where the high power laser spot is centered (alignment made with a CMOS camera, Thorlabs CMOS USB 2.0 Camera with 50 mm objective and extension ring). The different pyrometers have been calibrated by the manufacturer. The deviation between their reading in the measurement conditions (focus adjustment) and a black body source with 0.99 emissivity (ORIEL 67033) was measured to be lower than 2 K from 400 K to 1500 K. Above such temperatures the sensors accuracy is estimated as +/-2% of the temperature reading according to the manufacturer specifications. The black body source was also used for transmission measurements of the different vacuum viewports.

The setting of sample emissivity is the critical point and main source of uncertainty in the temperature measurement. In case of a monochromatic measurement, and under the marginal condition that the object temperature $T$ is much larger than the ambient temperature, the relative error made on the temperature as a function of the relative error on the emissivity can be directly derived from Planck's radiation law [16]:

$$\frac{e_T}{T} \approx \frac{\lambda T}{c_2}\frac{e_\varepsilon}{\varepsilon} \quad \text{Eq. (1)}$$

with T the temperature in K, $e_T$ the temperature error, $\lambda$ the measurement wavelength, $c_2$ the Planck's second radiation constant, $\varepsilon$ the emissivity and $e_\varepsilon$ the emissivity error.

In case of bichromatic measurements, only the emissivities ratio ($k_\varepsilon$) between the two wavelengths ($\lambda_1$, $\lambda_2$) is taken into account in the measurements, resulting in the following relative error made on the temperature measurement:

$$\frac{e_T}{T} \approx \left(\frac{\lambda_2\lambda_1}{\lambda_2-\lambda_1}\right)\frac{T}{c_2}\frac{e_{k\varepsilon}}{k\varepsilon} \qquad \text{Eq. (2)}$$

We will discuss the choice and evaluation of the emissivities in section III.

Eventually, a PID (Proportional, Integral, Derivative) feedback loop has been implemented to ensure well-controlled heating ramps and stable temperature set-points. It is based on the temperature measured with the pyrometer that is used as the input signal of a PID program controller (Sensortherm Regulus) that controls the laser power output (details in [13]). Figure 2 presents the case of a linear heating at 100 K/s up to 3600 K obtained on a graphite sample and the corresponding applied laser power.

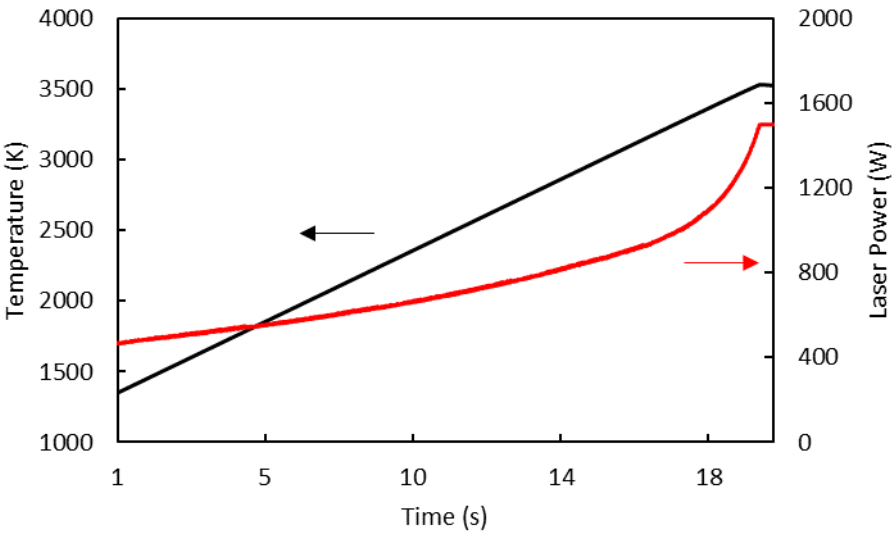


*Figure 2: Incident laser power and corresponding temperature evolution obtained on a graphite sample in case of a regulated linear ramp at 100 K/s.*

.

## III Simulations of Laser Graphite interactions

Graphite has advantaging properties for applications requiring high temperatures, in particular very high phase change temperature. At low ambient pressure, below 1 bar in our experimental conditions, graphite sublimates in its vapour phase at a temperature close to 4200 K [8]. Graphite is also characterized by a high thermal conductivity (above 100 W/m/K) at ambient temperature, an important parameter to consider in laser heating experiments. In addition to these elements, this material is characterized by excellent resistance to thermal shock, property which is extremely advantaging during laser heating experiments, which guarantees the integrity of the sample during sudden temperature drops (no damage to samples was noted during our experimental campaigns).

### a-Thermal properties of EDM3

Fine modelling of the laser / material interaction to calculate temperature gradients requires precise knowledge of the evolution of thermal properties with temperature. We describe in the following the thermophysical properties of EDM3 graphite that have been gathered from a bibliographical study.

For the apparent density of EDM3 we have used the value 1.79 g/cm$^3$ as reported in Ref. [12]. There is a decrease of the thermal conductivity with the temperature, going from 120 W/m/K at ambient temperature down to 40 W/m/K at 1900 K [12], with a non-linear behaviour as described in Figure 3. Above 1900 K the conductivity continues to decrease following an extrapolated profile that we have completed by means of our comparison experiment / simulations (more detailed are given in part IV). Also shown in Figure 3, is that the heat capacity of EDM3 graphite increases with increasing temperature, which is basically the same for all types of natural and manufactured graphite. Above 2300 K, heat capacity shows a slow increase and a simple extrapolation by power law has been used. Finally, we note that these properties of EDM3 are intrinsic to the graphite and apparently independent of density.

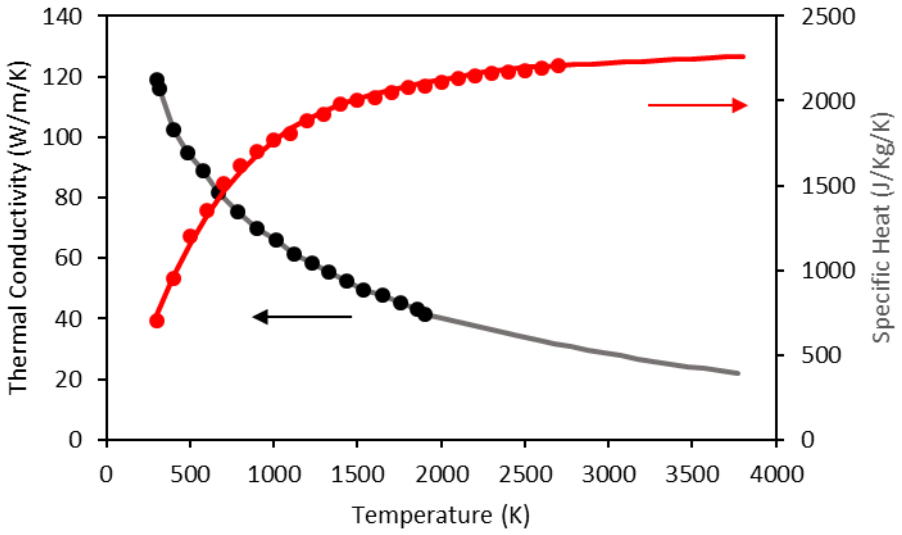


*Figure 3: Thermal Conductivity (K) and Specific Heat (Cp) of EDM3 graphite. Data points are extracted from [12], plain lines are extrapolated values used in this work (see equations in Appendix).*

b-Optical properties of EDM-3

The essential properties for the analysis and interpretation of laser heating experiments controlled by pyrometry are on the one hand the absorption at the wavelength of the laser, and on the other hand the emissivity at the wavelength of the pyrometers. These properties are highly dependent on the surface state (roughness, oxidation, etc.) and also depend on the temperature. Experiments must therefore necessarily go through a calibration step to determine these values in the experimental conditions (this step is detailed in part IV). Nevertheless, the values found in the literature constitute a starting point and we summarize below the available data.

The total emissivity of porous graphite has a value around 0.8-0.9, with dependencies on the surface state and porosity [17-22]. However, there are divergent results about the evolution of this emissivity with temperature as a function of different grades of porous graphite (values summarized in Figure 4). One of the available data source for POCO EDM-3 graphite reports the following equation between 1700 K to 2900 K [23]:

$$\varepsilon = 0.794 + (2.28 \times 10^{-5}) * T \qquad \text{Eq. (3)}$$

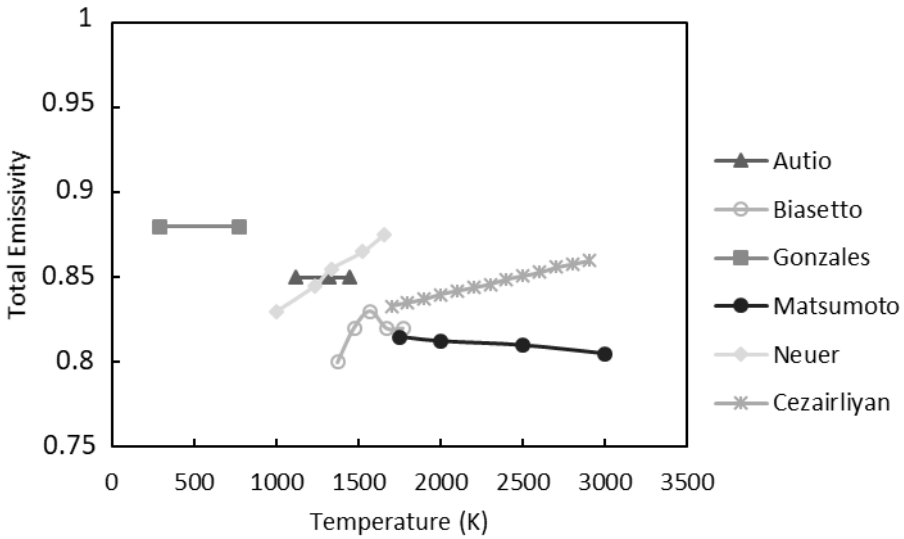


*Figure 4: Data from the literature of the total emissivity dependence on the temperature of porous graphite.*

We have reported in Figure 5 the spectral emissivity values of porous graphites, with properties close to EDM-3, around 1 µm (laser used in our experiments) [18,24-26], 1.5 µm (pyrometers used in our experiments) [18, 26, 27] and 0.65 µm [28,29] (different datasets available at this wavelength). It is difficult to identify clear trends in the temperature dependence except that the emissivity at 1-1.5 µm is higher than the total emissivity (in the range 0.85-0.95). We will come back to these points when we compare our values to those from the literature.

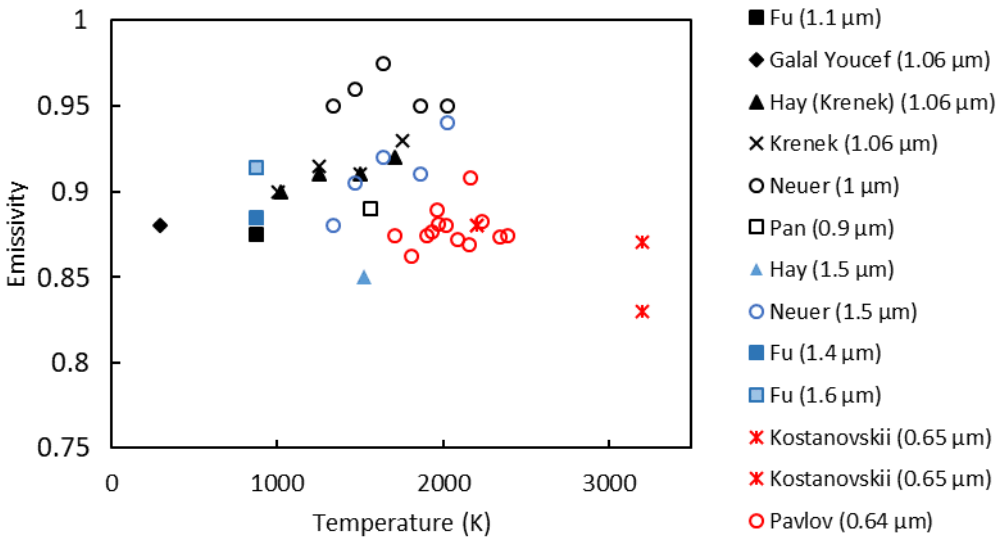


*Figure 5: Data from the literature on the spectral emissivity dependence on the temperature of porous graphite, for selected visible and NIR wavelengths.*

In addition to the aforementioned data, R. J. Papoular et al [30] provide values at different temperatures of the graphite extinction coefficient at our wavelengths of interest. At 300 K, the absorption coefficient has a value close to 1 in the near infrared. From this we consider that the absorption / emission of the radiation is purely a surface effect (penetration depth less than 100 nm).

## c- Numerical Model

Laser material interaction simulations have been conducted with a commercial software, COMSOL Multiphysics, which is based on the Finite Element Method. A 3D system is considered to model the samples in order to take into account possible non zero angles of incidence in the experiments. The non-linear heat flow equation (Eq. 4) is solved to obtain the temperature distribution and evolution T(x,y,z,t), considering conduction is the only heat transfer mechanism in the material.

$$\rho(T)C_p(T)\frac{\partial T}{\partial t} - \nabla \cdot (K(T) \cdot \nabla T) = 0 \quad , \qquad \text{Eq. (4)}$$

where ρ(T), $C_p$(T) and K(T) represent respectively, the density, the thermal conductivity and the specific heat for EDM3. The laser coupling in the material is approximated by surface absorption and is treated as an incoming heat flux S(x,y,z,t) expressed as:

$$S = A(T) I_N(x, y, z) \frac{P(t)}{\pi \omega^2} \qquad \text{Eq. (5)}$$

with A(T) the temperature dependent absorption (A=1-R with R the total reflectivity), $I_N$ the normalized distribution of the laser intensity on the sample surface ($I_n(x, y, z)=I(x,y,z)/I_{max}$), which takes into account the incidence, P(t) the laser power as a function of time and ω the waist of the incoming laser beam.

Radiation losses are taking into account as a surface boundary condition between the surface of the sample and the ambient air, taking into account ε(T) the total emissivity and its temperature dependence. Convection cooling is neglected in the simulations. Evaporative cooling is included as a surface boundary condition since it can be a significant heat transport mechanism as the temperature comes closer to the sublimation point. Based on the thermodynamics and the kinetic theory of gases, it is possible to evaluate the maximum rate of ejection (mass loss dm per unit of time dt and surface area dS) in a vacuum at any temperature T, as it is summarized in Ref. [31]:

$$\frac{dm}{dt dS} = \sqrt{\frac{M}{2\pi RT}} p_{sat} \qquad \text{Eq. (6)}$$

with M the molar mass of Carbon (12.011 g/mol), R the perfect gas constant and $p_{sat}$ the saturating vapour pressure. This last parameter is obtained under the perfect gas assumption, neglecting vapour redeposition, radial gradient effects, formation of different Carbon species, or oxidation, but it should give an upper limit on the ejection rate. $p_{sat}$ can be obtained with the Clausius-Clapeyron relation considering:

$$p_{sat} = p_0 exp\left[\frac{\Delta H}{R}\left(\frac{1}{T_v} - \frac{1}{T}\right)\right] \qquad \text{Eq. (7)}$$

with ΔH the enthalpy of the phase change and $T_v$ the temperature of the phase change at initial pressure $p_0$. By introducing in the right hand side of Eq. (6) a coefficient β (which is smaller than unity) we can empirically take into account the various factors lowering the evaporation rate. The outgoing heat flux at the boundary can then be obtained as:

$$\varphi(T) = \frac{dm}{dtdS}\frac{\Delta H}{R} = \beta\sqrt{\frac{M}{2\pi RT}}\frac{\Delta H}{R}p_0 exp\left[\frac{\Delta H}{R}\left(\frac{1}{T_v}-\frac{1}{T}\right)\right] \qquad \text{Eq. (8)}$$

To evaluate the importance of different losses mechanisms, we have compared on Figure 6 the results of the simulations under different assumptions, with or without losses by radiation and evaporation in typical conditions of our experiments (β = 1). It can be established from these numerical results that above 2300 K, radiation losses are required to obtain a good description of the temperature evolution. Above 3300 K however, in the range of temperatures that interest us, it is required to introduce the heat losses by evaporation that become significant.

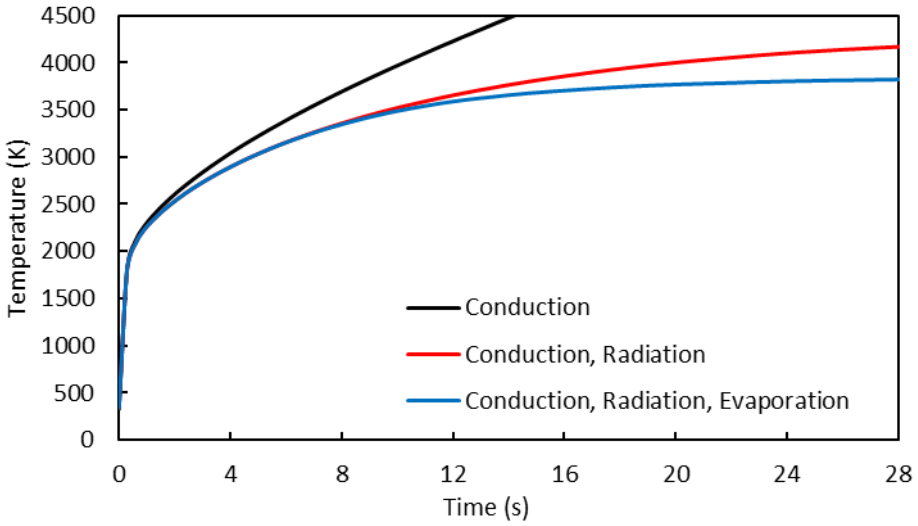


*Figure 6: Temperature evolution on a porous graphite sample, 30mm diameter and 10 mm thickness, submitted to a 1500 W continuous laser illumination, with 5 mm diameter at 1/e². The temperature is plotted at the surface center, on the side illuminated by the laser. Calculation is done under various hypothesis, as discussed in the text.*

## IV Results and discussion

The methodology that has been followed during this work was to progressively increase the temperature investigated. In this way, access to high temperatures was conditioned to the validation of instrumentation and simulation at lower temperatures. In the report of our results we have therefore separated the ranges of investigation between “moderate temperature”, i.e. below 1500 K for which standard thermocouples can be used, “high temperature”, i.e. below 2800 K the onset of material removal, and “very high temperatures”, i.e. above 2800 K.

### a- Elevated temperatures (<1500 K)

The sample used for this first set of experiments is an EDM3 disk, of 34 mm diameter and 10 mm thickness. It has been instrumented with 2 type C thermocouples (TC) embedded in the sample through drilled holes. Thermal contact and stabilization of the thermocouples was ensured with a thermally conductive glue. The positions of the TC have been measured with X-ray radiography and are illustrated in Figure 7. The temperature calculated with the numerical model can then be extracted at these exact positions for comparison with the experiments (note that the thermocouples are not taken into account in the model). The surface temperature is measured with the bichromatic pyrometer operating in the 850-1700 K temperature range. Three independent temperature measurements are obtained with this system: a first one corresponding to the 1.45-1.65 µm range (C1), a second to the 1.65-1.8 µm range (C2), and a third one corresponding to the bichromatic measurement (B). This pyrometer is pointing at the sample center, with an estimated accuracy of +/- 1 mm. Additionally the thermal camera is used to record simultaneously the temperature on the sample surface (CamIR). Therefore 6 measurements were available for these experiments (TC1, TC2, C1, C2, B and CamIR).

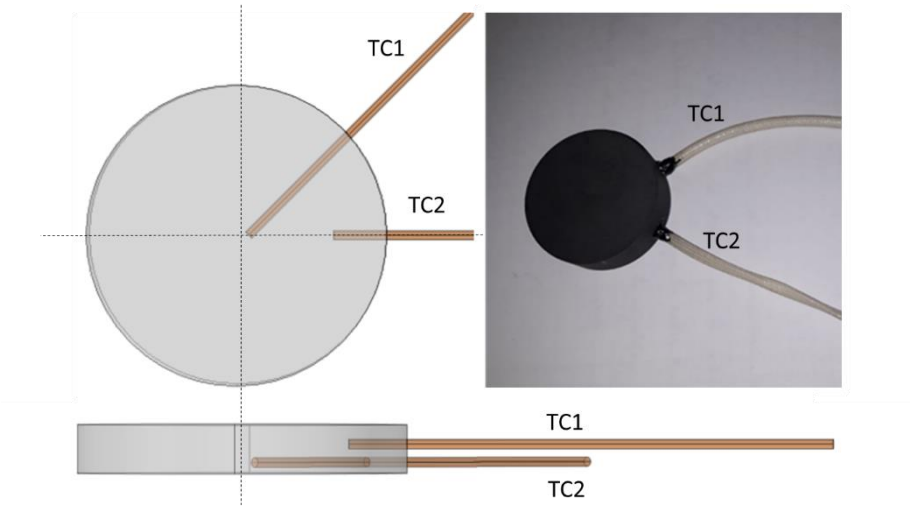


*Figure 7: Schematic of the sample instrumented with two thermocouples (TC1 and TC2) and their respective positions. A picture of the sample is also shown. TC1 is 3 mm below the surface and 11 mm from the center. TC2 is 1 mm below the surface and 1.5 mm from the center.*

Simple experiments have been first conducted: a collimated Gaussian laser beam (13.5 mm diameter at $1/e^2$) is directed on the center of the sample surface at normal incidence, with a constant power P for an amount of time. The signal is recorded on the different sensors and we have set the emissivities values of C1, C2, B to obtain the same temperature on the three channels. This was done with some post-processing on the acquired data sets. Considering the theoretical emission of a black body or a grey body as graphite, only one set of values is possible. The camIR emissivity (0.68) was then adjusted to obtain the same temperature. Signals TC1 and TC2 were considered as calibrated. Following this procedure for different temperatures it was possible to obtain the emissitivies at the operating wavelengths of our sensors. In the temperature range explored with this sample, the emissivities obtained for C1 and C2 were 0.9, and an emissivity ratio for channel B of 1. These values are in close agreement to the reported ones in Figure 6. An example of experimental results and their comparison to the simulated values is given in Figure 8.

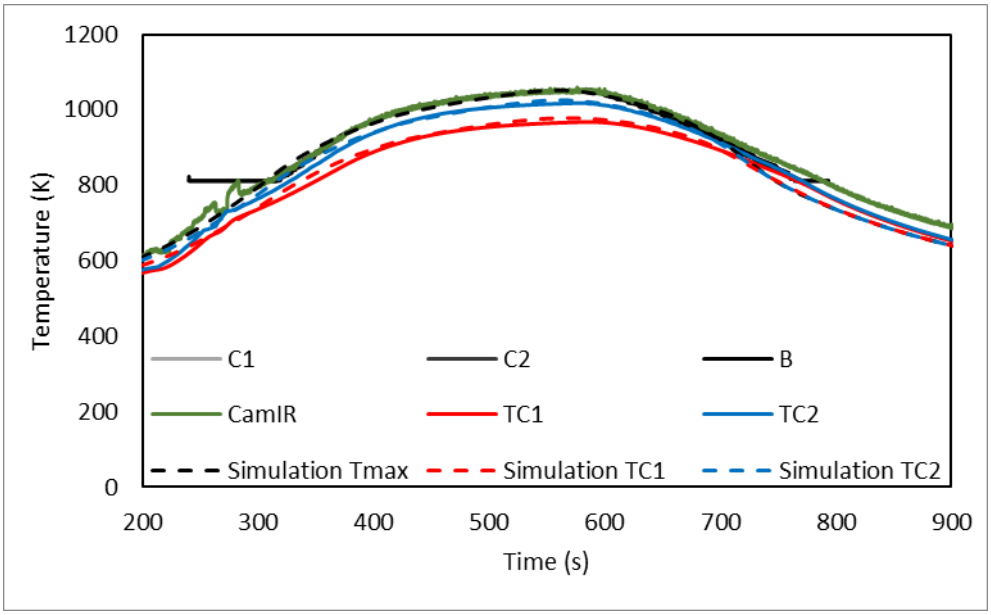


*Figure 8: Data recorded with the different probes (pyrometer, thermal camera and thermocouples) during a laser heating sequence on the calibrated sample, and their comparison with the simulations. C1: pyrometer channel 1 (*1.45-1.65 µm*) ; C2: pyrometer channel 2 (*1.65-1.8 µm) ; B: Bichromatic channel of pyrometer ; CamIR: maximum temperature from the thermal camera ; TC1 : first thermocouple ; TC2 : second thermocouple ; "Simulation Tmax" is the temperature predicted by your model at the centre of the laser heated face

Based on the measured absorption values and taking into account the thermal properties of EDM-3 graphite described in the previous section we have obtained an excellent agreement between experiments and simulations, as shown in the example of Figure 8. The set of thermal and optical parameters used in the simulations is therefore a good starting point to explore the behaviour of graphite at higher temperatures.

### b- High Temperature laser heating (1500 K<T<2800 K)

Based on the previously described calibration experiments performed at moderate temperature, we were able to set the optical instruments (pyrometer and thermal camera) to obtain accurate temperature values, supported by numerical simulations. For higher temperature however, samples instrumented with thermocouples were not available and we have worked only with the pyrometers

and the thermal camera, following the procedures described in the previous section to set the emissivity values. These settings were done on temperature plateaux up to 2800 K and repeated several times to check the reproducibility. An example of laser heating experiment with the recording of the different measurement systems is shown on Figure 9.

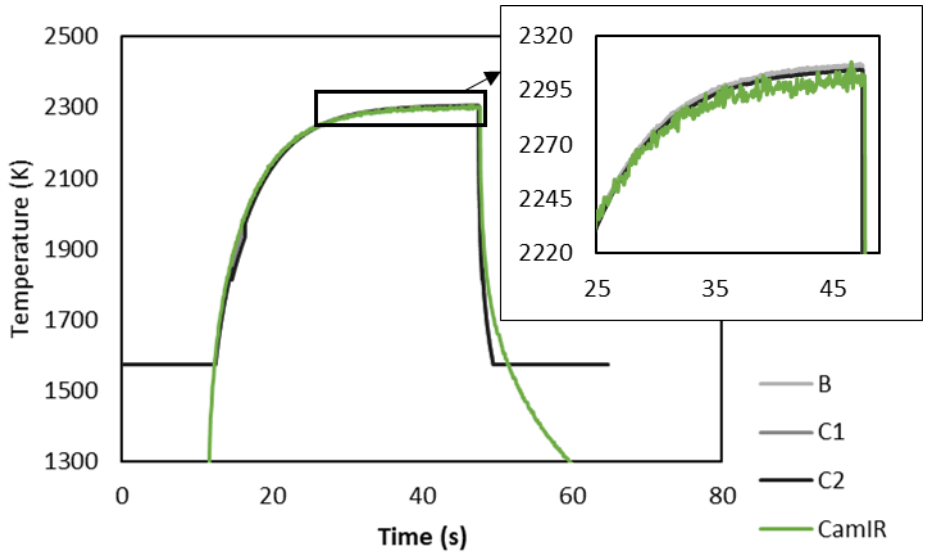


*Figure 9: Laser heating experiment on a graphite disk sample (diameter 30 mm and thickness 3 mm) with 675 W of laser power. The minimum temperature measured with the pyrometer (C1, C2 and B) is 1600 K. The inset of the upper right shows that the signal difference between the sensors is less than 10 K at 2300 K.*

The emissivities obtained following this protocol are reported in Table 1, as the relative error on their determination and the corresponding temperature uncertainties. They are compared on Figure 10 to the different values reported in the literature for spectral emissivity around 1.5 µm. We claim that following our protocol the temperature can be determined within 1% accuracy at 2800 K with monochromatic measurements, and 2% in case of bichromatic measurement. This latter measurement, even if less accurate, is particularly useful in case of material ejection and possible signal attenuation by scattering and absorption in the vaporized material, assuming that both channels are attenuated by the same amount since the two wavelengths are close.

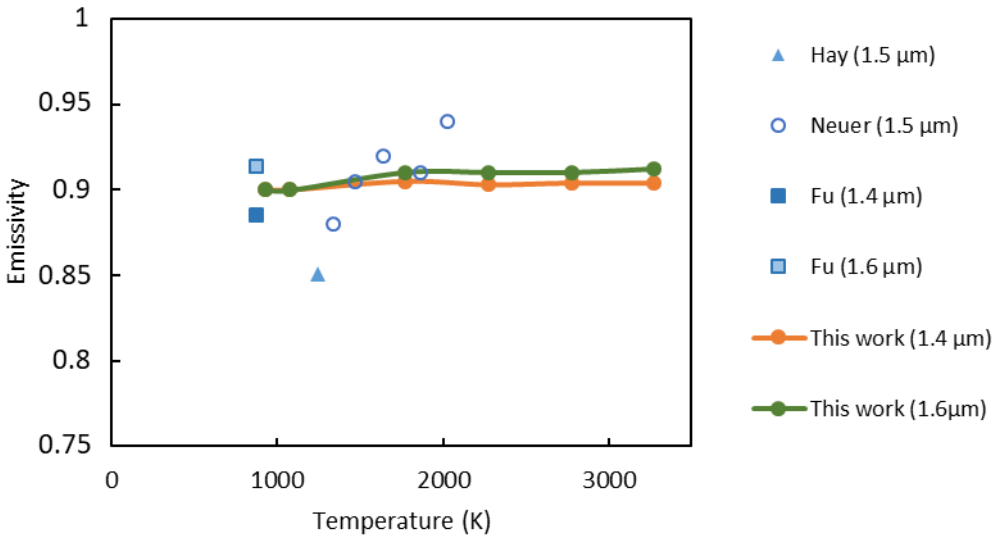


*Figure 10: Comparison with data from the literature of spectral emissivity dependence on the temperature of porous graphite obtained in this work.*

Table 1: The determined emissivities and their ratio at different temperatures on Graphite EDM3. The absolute temperature error ($e_T$) is determined by equations (1) and (2) with an additional error based on the pyrometer specification from the manufacturer (0.5% x T).

| Temperature | $\varepsilon_1$ (1,4µm) | $e_T$ | $\varepsilon_2$ (1,6µm) | $e_T$ | $k_\varepsilon$ | $e_T$ |
|---|---|---|---|---|---|---|
| 1800 K | 0.91+/-0.002 | 10 K | 0.900+/-0.002 | 10 K | 0.989+/-0.005 | 21 K |
| 2300 K | 0.907+/-0.002 | 12 K | 0.903+/-0.002 | 13 K | 0.996+/-0.005 | 32 K |
| 2800 K | 0.912+/-0.002 | 16 K | 0.905+/-0.002 | 16 K | 0.992+/-0.005 | 44 K |

Following these calibration results we have proceeded to laser heating experiments at high temperature with a simple procedure: the laser power was set to a constant value, from 300 to 1100 W and applied for few tens of seconds. The temperature was measured with the pyrometer at the center of the face exposed to the laser flux. Results are reported on Figure 11 for different applied powers and different irradiation conditions, both from the experiments and from simulations

conducted with the same input parameters (measured laser power, beam diameter and angle of incidence).

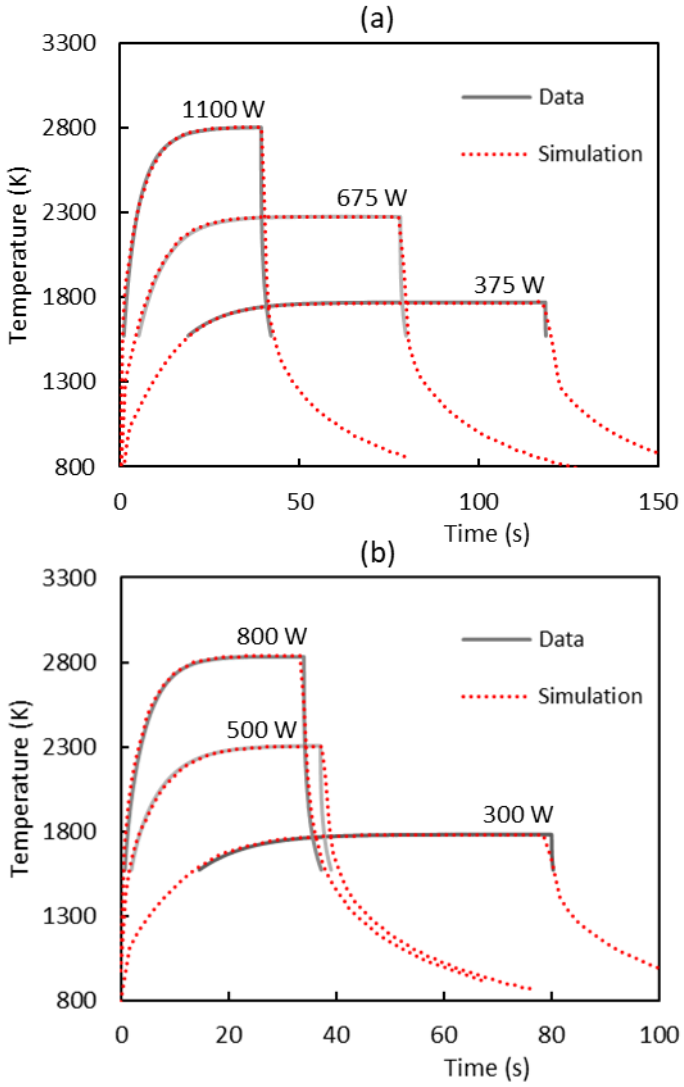


Figure 11: Results of different laser heating experiments with the maximum temperature measured at the front face (from bichromatic pyrometer). (a) Laser beam diameter of 13.5 mm and 0° angle of incidence; (b) Laser beam diameter of 8 mm and 45° angle of incidence.

To obtain such results we have extended the thermal conductivity for T > 1873 K, with the following function:

$$K(T) = 42 - 20\frac{T-1873}{1400} + \frac{(T-1873)^2}{500000} \text{ for T>1873 K} \qquad \text{Eq. (9)}$$

In such conditions we have obtained very consistent results for diverse laser exposure conditions, as shown on Figure 11, which validate the thermal model up to 2800 K.

### c-Very high temperature laser heating (> 2800 K)

For very high temperatures (approaching 3300 K) it was not experimentally possible to heat the sample at the target temperature for long durations as in the previous section, because of significant mass loss and pollution of the experimental chamber. We have worked with another methodology consisting in regulating the laser power to increase the temperature at a constant rate and reach the targeted temperature, as described in section II. Figure 12 shows 3 experiments where temperatures up to 3400 K, 3600 K and 3800 K (respectively) have been reached with a linear heating rate of 100 K/s during 30 s. At the end of the heating sequence the laser was shut-down resulting in very fast cooling rate of the sample: 1300 K temperature drop in 0.1 s.

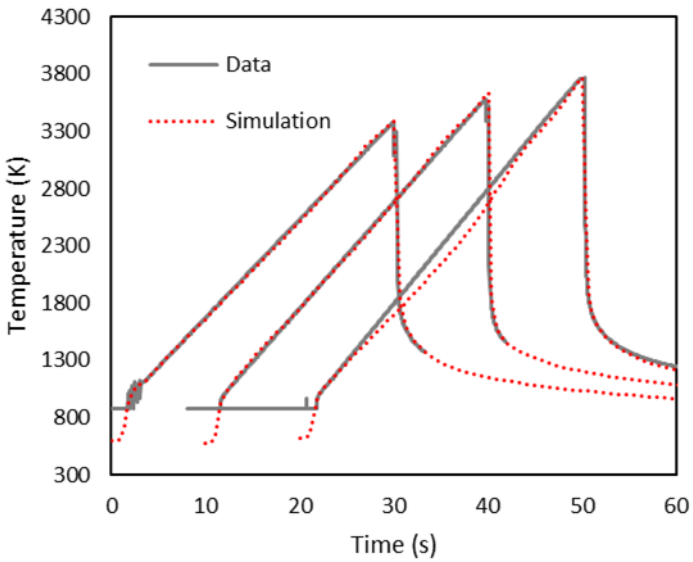

*Figure 12: Laser heating experiments up to very high temperature with a linear heating rate and their comparison to simulations. Laser beam diameter of 4 mm (Super-Gaussian function of power 6) and 40° angle of incidence, measurements done with the monochromatic pyrometer.*

Numerical simulations were conducted taking into account the recorded laser power as a function of time for each experiment. The decreasing thermal conductivity with temperature described in Eq (2) was used and the β coefficient was adjusted to 0.1 to obtain a good description of the experimental data. Higher values of β lead to higher losses by evaporation and an underestimation of the temperatures above 3300 K with the model. Additionally, we point out that since the position of the studied sites was not necessarily at the center of the sample (several test sites were done per sample), only a 3D simulation taking into account the exact position of the sites is able to give an accurate description of the experimental data. The sample holder has also to be taken into account in the simulations.

On this basis very consistent descriptions of the experimental data are obtained, under different exposure conditions (laser spot size, position on the sample). However we would like to point out that a slightly different conductivity function associated to other value of β (or a temperature dependent β function) could have led to similar results. Only a very extensive study could help to refine these parameters. However, this value of β=0.1 is consistent with reported evaporation coefficient of graphite [32,33]

To simulate the crater formation, we have taken into account in the numerical model the velocity of the evaporation front at the sample surface, given by [31]:

$$v(T) = \beta\sqrt{\frac{M}{2\pi RT}}\frac{p_{sat}(T)}{\rho(T)} \qquad \text{Eq (10)}$$

To investigate the crater formation dynamic, we have used a moving boundary condition at the sample surface, controlled by the local evaporative velocity, associated with a moving mesh functionality in the 3D numerical model.

Above 3300 K significant mass losses were observed, leading to crater formation in the laser heated area. The crater morphologies have been measured thanks to our profilometer (type VEECO) and then compared with our simulations. An example of such an analysis is given on Figure 13 with a 3D mapping and extractions of maximum depth profiles following the white dashed lines. This example of a calculated crater compared to experimental measurements shows a very consistent result.

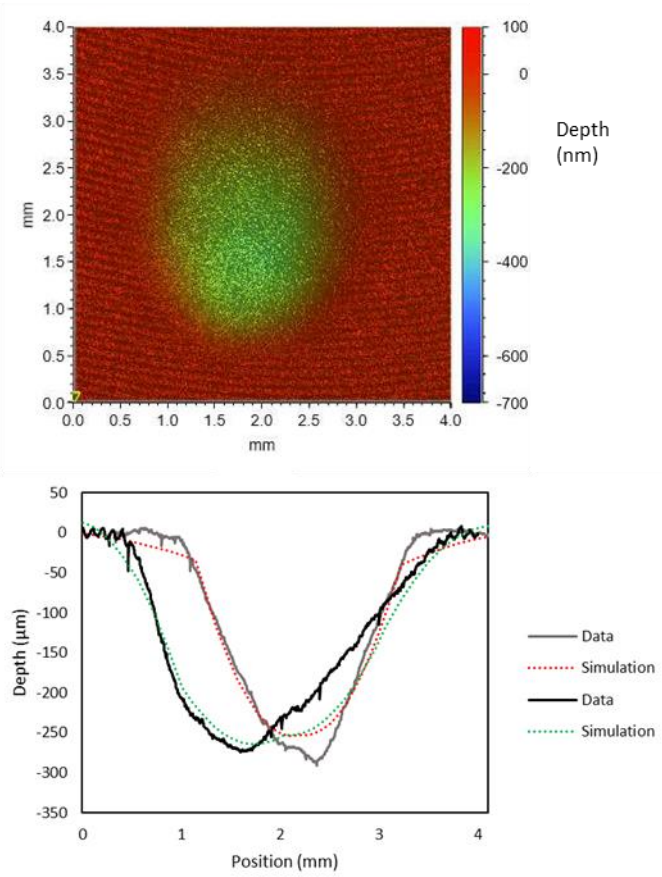


*Figure 13: Crater observed on a graphite sample after reaching 3800 K in the heating conditions described on Figure 12. Top: 3D-map of the optical profilometer measurement; Bottom: Vertical and Horizontal extraction of depth profiles (the larger one is on the vertical axis), and their comparison to simulation results.*

The same characterization has been done for the other craters coming from the tests presented on Figure 12. Then we have extracted for each crater the experimental maximum depth to compare it

with simulations as shown in Figure 14. These results give us confidence in the choice of the estimated values of the parameters used in the model (mainly K(T) and β).

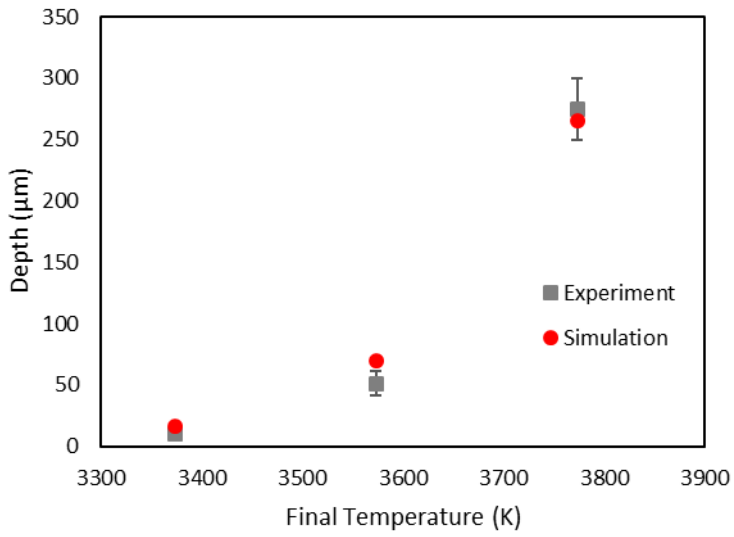


*Figure 14: Comparison of measured and calculated depth of laser-induced craters on graphite. The results are reported as a function of the final temperature reached during a linear heating rate such as shown on Fig. 12.*

## V Conclusion

The objective of this work was to study laser graphite interactions at very high temperature to obtain a comprehensive description of the temperature gradients and material removal mechanisms. To do so, a better knowledge of the properties of graphite at such temperatures is required. For that purpose, laser-based experiments and associated instrumentation have been developed as shown in this paper. We have demonstrated the ability of our experimental set-up to perform controlled heating on graphite above 3300 K with well-controlled heating rates. This experimental part of our work was based on the implementation of robust calibration protocols to determine the spectral emissivity

values of graphite, that were obtained over an extended temperature range. A 3D numerical model has also been developed based on the Finite Element Method to analyse the experimental results and to derive the properties of interest by comparing experimental data to simulation results. Very satisfactory results were obtained on the heating and cooling phases up to 3800 K based on the thermal conductivity function we have introduced, and taking into account evaporation cooling. An estimation of the evaporation coefficient of graphite was also obtained that gives consistent results for the description of temperature gradients and crater formations above 3300 K. This work can be used as the stepping-stone for more detailed studies of the graphite behaviour at very high temperature, such as the mechanical behaviour. The approach applied on graphite could be also applied to other high temperature materials, however in that case the instrumentation should be adapted (choice of pyrometers and laser wavelengths based on the optical properties of the material investigated).

## Data Availability Statement

The data that supports the findings of this study is available from the corresponding author upon request.

# Bibliography

[1] Graphite for High Temperature Gas-Cooled Nuclear Reactors, Published by The American Society of Mechanical Engineers, STP-NU-009 – 2008 (2008)

[2] D. Liu, B. Gludovatz, H. S. Barnard, M. Kuball, R. O. Ritchie, 'Damage tolerance of nuclear graphite at elevated temperatures', Nature Communications 8, 15942 (2017).

[3] X.-W. Zhou, Y.-P. Tang, Z.-M Lu, J. Zhang, B. Liu, 'Nuclear graphite for high temperature gas-cooled reactors', New Carbon Materials 32, 193 (2017).

[4] C. H. Skinner, C. A. Gentile, G. Guttadora, A. Carpe, S. Langish, K. M. Young, M. Nishi, W. Shu, 'Tritium Removal by Laser Heating and Its Application to Tokamaks', Fusion Science and Technology 41, 716 (2002).

[5] A. Semerok, Sv. Fomichev, J.-M. Weulersse, F. Brygo, P.-Y. Thro, C. Grisolia, 'Heating and ablation of tokamak graphite by pulsed nanosecond Nd-YAG lasers', Journal of Applied Physics 101, 084916 (2007).

[6] A Goriaev, T Wauters, R Brakel, S Brezinsek, A Dinklage, J Fellinger, H Grote, D Moseev, S Sereda, O Volzke and W7-X team, "Wall conditioning at the Wendelstein 7-X stellarator operating with a graphite divertor", Physica Scripta 2020, 014063 (2020)

[7] H. O. Pierson, 'Handbook of Carbon, Graphite, Diamond and Fullerenes: Properties, Processing and Applications', William Andrew Publishing (1993)

[8] F.P. Bundy, 'Pressure-Temperature phase diagram of elemental carbon', Physica A 156, 169 (1969).

[9] P. Combis, P. Cormont, L. Gallais, D. Hebert, L. Robin, J.-L. Rullier, 'Evaluation of the fused silica thermal conductivity by comparing infrared thermometry measurements with two-dimensional simulations,' Applied Physics Letters 101, 211908 (2012).

[10] S. Elhadj, M. J. Matthews, S. T. Yang, 'Combined Infrared Thermal Imaging and Laser Heating for the Study of Materials Thermophysical and Processing Properties at High Temperatures', Critical Reviews in Solid State and Materials Sciences 39, 17 (2014).

[11] I. L. Shabalin, 'Ultra-High Temperature Materials', Springer Netherlands (2014).

[12] Poco Graphite, Inc. "Properties and Characteristics of Graphite for the EDM Industry", Edited by R. G. Sheppard, Dwayne Morgan, D. M. Mathes, D. J. Bray, 5th Printing (2002).

[13] M. Minissale, A. Durif, P. Hiret, T. Vidal, J. Faucheux, M. Lenci, M. Mondon, G. Kermouche, Y. Pontillon, C. Grisolia, M. Richou, L. Gallais 'A high power laser facility to conduct annealing tests at high temperature', Review of Scientific Instruments 91, 035102 (2020).

[14] T. Vidal, L. Gallais, J. Faucheux, H. Capdevila, J. Sercombe, Y. Pontillon, 'Simulation of Reactivity Initiated Accident thermal transients on nuclear fuels with laser remote heating', Journal of Nuclear Materials 530, 151944 (2020).

[15] B. Aubert, D. Hebert, J.L. Rullier, E. Lescoute, L. Videau, and L. Berthe, 'Simulation of laser-driven cratering experiments on aluminum', Journal of Laser Applications 31, 042014 (2019).

[16] F. Cabannes, 'Pyrométrie Optique', Techniques de l'Ingénieur, R2610 V1 (1990)

[17] G.W. Autio, E. Scala, 'The normal spectral emissivity of isotropic and anisotropic materials', Carbon 4, 13 (1966)

[18] G. Neuer, 'Spectral and Total Emissivity Measurements of Highly Emitting Materials', International Journal of Thermophysics 16, 257 (1995)

[19] T. Matsumoto, A. Onon, 'Specific Heat Capacity and Emissivity Measurements of Ribbon-Shaped Graphite Using Pulse Current Heating', Int J Thermophys 16, 267 (1995)

[20] L. Biasetto, M. Manzolaro, A. Andrighetto, 'Emissivity measurements of opaque gray bodies up to 2000 ◦C by a dual-frequency pyrometer', European Physical Journal A 38, 167 (2008)

[21] F. Wang, L. Cheng, H. Mei, Q. Zhang, L. Zhang, 'Effect of Surface Microstructures on the Infrared Emissivity of Graphite', International Journal of Thermophysics 35, 62 (2014)

[22] A.E. Gonzales, N.C. Herr, G.P. Perram, 'Experimental study of laser irradiated graphite oxidation using IFTS', Combustion and Flame 192, 180 (2018)

[23] A. Cezairliyan, F. Righini, 'Measurements of Heat Capacity, Electrical Resistivity, and Hemispherical Total Emittance of Two Grades of Graphite in the Range of 1500° to 3000°K by a Pulse Heating Technique,' Revue Internationale des Hautes Températures et des Réfractaires 12, 128 (1975).

[24] S. Galal Yousef, P. Sperfeld and J. Metzdorf, 'Measurement and calculation of the emissivity of a high-temperature black body', Metrologia, 37 365-368 (2000).

[25] S. Krenek, D. Gilbert, K. Anhalt, D.R. Taubert, J. Hollandt, 'A Dynamic Method to Measure Emissivity at High Temperatures', International Journal of Thermophysics 1866-7 (2014).

[26] T. Fu, M. Duan, J. Tang, C. Shi, 'Measurements of the directional spectral emissivity based on a radiation heating source with alternating spectral distributions', International Journal of Heat and Mass Transfer 90, 1207 (2015).

[27] B. Hay, K. Anhalt, L. Chapman, K. Boboridis, J. Hameury, S. Krenek, L. Vlahovic, N. Fleurence, and O. Beneš, 'Traceability Improvement of High Temperature Thermal Property Measurements of Materials for New Fission Reactors', IEEE Transactions on Nuclear Science 61, 2112 (2014).

[28] A. V. Kostanovskii, M. G. Zeodinov, and M. E. Kostanovskaya, 'The Determination of Thermal Conductivity and Emissivity of Graphite at High Temperatures', High Temperature 43, 793–795 (2005).

[29] T. Pavlov, L. Vlahovic, D. Staicu, R.J.M. Konings, M.R. Wenman, P. Van Uffelen, R.W. Grimes, 'A new numerical method and modified apparatus for the simultaneous evaluation of thermo-physical properties above 1500 K: A case study on isostatically pressed graphite', Thermochimica Acta 652, 39-52 (2017).

[30] R. J.Papoular and R. Papoular, ‘Some Optical Properties of graphite from IR to millimetric wavelengths’, Monthly Notices of the Royal Astronomical Society MNRAS 443, 2974-2982 (2014).

[31] L. Robin, P. Combis, P. Cormont, L. Gallais, D. Hebert, C. Mainfray, J.-L. Rullier, ‘Infrared thermometry and interferential microscopy for analysis of crater formation at the surface of fused silica under $CO_2$ laser irradiation’, Journal of Applied Physics 111, 063106 (2012).

[32] L. Brewer, P.l W. Gilles, F. A. Jenkins, ‘The Vapor Pressure and Heat of Sublimation of Graphite’, The Journal of Chemical Physics 16, 797 (1948).

[33] R. P. Burns, A. J. Jason, M. G. Inghram, ‘Evaporation Coefficient of Graphite’, The Journal of Chemical Physics 40, 1161 (1964).

# Appendix: Thermal and optical properties of amorphous graphite used in this work.

- Absorption (at 1070 nm)

0.875 for T < 500 K, 0.875+0.015x((T-200)/700) for 500 K < T < 2000 K, 0.914 for T > 2000 K Eq. (A1)

- Density (kg/m$^3$):

$\rho(T)=1749.6-0.031918xT-3.7643x10^{-6}*T^2-1.0321x10^{-9}xT^3+2.3581x10^{-13}xT^4$ Eq. (A2)

- Evaporation rate (in m.s$^{-1}$)

$$v(T) = \beta \frac{P_0}{\rho(T)} \sqrt{\frac{M}{2\pi RT}} exp\left(\frac{U}{R}\left(\frac{1}{T_v} - \frac{1}{T}\right)\right)$$ Eq. (A3)

with β=0.1, M=12 g.mol$^{-1}$, $T_v$ = 4300 K, U = 703 KJ.mol$^{-1}$ and ρ(T) expression given in this appendix.

- Specific Heat (J/kg/K)

$C_p(T)=-159.87+3.6550xT-2.3805\ x10^{-3}xT^2+7.3827x10^{-7}xT^3-8.7978x10^{-11}xT^4$ for 293 K < T < 2500 K Eq. (A4)

$C_p(T)= 2198.09+0.05x(T-2500)$ for T > 2500 K Eq. (A5)

- Thermal Conductivity:

$K(T)=120.5-0.1488x(T-273.15)+1.552x10^{-4}x(T-273.15)^2-9.153x10^{-8}x(T-273.15)^3+2.093x10^{-11}x(T-273.15)^4$ for 293 K < T < 1873 K Eq. (A6)

$K(T)=42-20x(T-1873)/1400+((T-1873)^2)/500000$ for T> 1873 K Eq. (A7)

- Total emissivity

$\varepsilon(T)=0.794+2.28x10^{-5}xT$ for 293 K < T < 3500 K Eq. (A8)